Sio-Iong Ao
Len Gelman
Haeng Kon Kim *Editors*

Transactions on Engineering Technologies

World Congress on Engineering 2019

Springer

Transactions on Engineering Technologies

Sio-Iong Ao · Len Gelman · Haeng Kon Kim
Editors

Transactions on Engineering Technologies

World Congress on Engineering 2019

Springer

Editors
Sio-Iong Ao
International Association of Engineers
IAENG Sectretariat
Hong Kong, Hong Kong

Len Gelman
University of Huddersfield
Huddersfield, UK

Haeng Kon Kim
School of Software Convergence
Daegu Catholic University
Daegu, Korea (Republic of)

ISBN 978-981-15-8272-1 ISBN 978-981-15-8273-8 (eBook)
https://doi.org/10.1007/978-981-15-8273-8

This Springer imprint is published by the registered company Springer Nature Singapore Pte Ltd.
The registered company address is: 152 Beach Road, #21-01/04 Gateway East, Singapore 189721, Singapore

Preface

A large international conference on Advances in Engineering Technologies and Physical Science was held in London, UK, July 3–5, 2019, under the World Congress on Engineering 2019 (WCE 2019). The WCE 2019 is organized by the International Association of Engineers (IAENG); the Congress details are available at: http://www.iaeng.org/WCE2019. IAENG is a non-profit international association for engineers and computer scientists, which was founded originally in 1968. The World Congress on Engineering serves as good platforms for the engineering community to meet with each other and to exchange ideas. The conferences have also struck a balance between theoretical and application development. The conference committees have been formed with over 300 committee members who are mainly research center heads, faculty deans, department heads, professors, and research scientists from over 30 countries. The congress is truly global international event with a high level of participation from many countries. The response to the Congress has been excellent. There have been more than 300 manuscript submissions for the WCE 2019. All submitted papers have gone through the peer-review process, and the overall acceptance rate is 50.93%.

This volume contains 18 revised and extended research articles written by prominent researchers participating in the conference. Topics covered include mechanical engineering, engineering mathematics, computer science, electrical engineering, and industrial applications. The book offers the state of the art of tremendous advances in engineering technologies and physical science and applications, and also serves as an excellent reference work for researchers and graduate students working on engineering technologies and physical science and applications.

Hong Kong — Sio-Iong Ao
Huddersfield, UK — Len Gelman
Daegu, Korea (Republic of) — Haeng Kon Kim

Contents

About the Editors

Dr. Sio-Iong Ao finished his doctoral research at The University of Hong Kong and postdoctoral researches at the University of Oxford and Harvard University and is a former Visiting Professor of Cranfield University, UK, and University of Wyoming, USA.

Prof. Len Gelman, Ph.D. Dr. of Sciences (Habilitation) joined Huddersfield University as Professor, Chair in Signal Processing/Condition Monitoring and Director of Centre for Efficiency and Performance Engineering, in 2017, from Cranfield University, where he worked as Professor and Chair in Vibro-Acoustical Monitoring since 2002.

Len developed novel condition monitoring technologies for aircraft engines, gearboxes, bearings, turbines, and centrifugal compressors.

Len published more than 250 publications, 17 patents and is co-editor of 11 Springer books.

He is Fellow of: BINDT, International Association of Engineers and Institution of Diagnostic Engineers, Executive Director, International Society for Condition Monitoring, Honorary Technical Editor, International Journal of Condition Monitoring, Editor-in-Chief, International Journal of Engineering Sciences (SCMR), Chair, annual International Condition Monitoring Conferences, Honorary Co-Chair, annual World Congresses of Engineering, Co-Chair, International Conference COMADEM 2019 and Chair, International Scientific Committee of Third World Congress, and Condition Monitoring.

He was General Chair, First World Congress, Condition Monitoring, Chair, Second World Congress, Engineering Asset Management and Chair, International Committee of Second World Congress, Condition Monitoring.

Len is Chair of International CM Groups of ICNDT and EFNDT and Member of ISO Technical Committee, Condition Monitoring.

Len made 42 plenary keynotes at major international conferences. He was Visiting Professor at ten universities abroad.

Prof. Haeng Kon Kim is Vice President of Research and Information, Dean of engineering college, and Professor in the Department of Computer Engineering Catholic University of Daegu, Korea. He has been a research staff member in Bell Labs and NASA Center in USA. Professor Kim is Chief Editor of KIPS SE-Sig journal and Korea Multimedia Society, an editorial board of Korea Information Science Society (KISS) and a steering committee of Korea Information Processing Society (KIPS).

Numerical Investigation of an Unmanned Aircraft Vehicle (UAV) Using Fluid-Structure Interaction

Kevin Marangi and Salim Mohamed Salim

Abstract This study employed Fluid-Structure Interaction (FSI), which is the coupling of Computational Fluid Dynamics (CFD) with Finite Element Analysis (FEA), to investigate the structural consequences of a wind gust on an Unmanned Aircraft Vehicle (UAV). The wind gust is modelled as a sudden increase to 23 ms^{-1} in airspeed when the UAV is initially cruising at a velocity of 13 ms^{-1}. In the first step, CFD simulations were carried out using ANSYS FLUENT, and validated against XFLR5 (an open-source software based on Massachusetts Institute of Technology (MIT)'s low Reynolds number CFD program, XFOIL). A steep increase in aerodynamic loads is observed as a result of the wind gust. The values jumped to 244 N for lift and 13.2 N for drag compared to 77.2 and 4.34 N during normal cruise flight conditions. In the next stage, the CFD-obtained pressure fields were exported to ANSYS MECHANICAL to run a structural analysis of the wings' response to the induced aerodynamic load. A slender component connecting the back-wing's outer shell and spar, experienced the largest maximum stress of 75.0 MPa, which amounts to a threefold increase from 23.8 MPa during normal flight conditions. In the final step, the FEA numerical results are analytically calculated to determine the structural response of the wing-fuselage connectors. The entire investigation concludes that, although larger aerodynamic loads, and consequently larger stresses are generated due to an increase in wind speed (mimicking a sudden wind gust), the UAV's structural integrity remains intact.

Keywords Aerodynamic loads · CFD · Fluid-structure interaction · Turbulence · UAV · Composite materials · Canard wing configuration

K. Marangi (✉)
Department of Mechanical Engineering, School of Engineering, EPFL, Route Cantonale, 1015 Lausanne, Switzerland
e-mail: marangikevin1@gmail.com

S. M. Salim
College of Engineering, Swansea University, Swansea SA1 8EN, UK
e-mail: s.m.salim@swansea.ac.uk

S.-I. Ao et al. (eds.), *Transactions on Engineering Technologies*,
https://doi.org/10.1007/978-981-15-8273-8_1

1 Introduction

UAVs have become central players in an increasing number of civilian applications despite originally being developed for military use. The Institution of Mechanical Engineers (IMechE) has introduced a competition that challenges university students to design and build a UAV, which could be deployed to assist during disasters. University of Dundee's engineering student team, *Haggis Aerospace*, participated in this competition and designed the UAV in Fig. 1. This UAV featured a *lifting canard wing configuration*, which is a non-traditional aircraft wing configuration. In this arrangement, the smaller flying surfaces, called *canard wings*, are located before the main wing in order to contribute to the total lift generated. It is worth noting that in the conventional wing setup, the larger wing is in front of the smaller flying surface, which is generally used for aircraft control rather than for lift generation.

The student team employed XFL5 software as a CFD tool for designing their UAV, as XFLR5 is based on MIT's famous XFOIL program and is also open source. Due to the additional manner of generating lifting forces in this wing arrangement, it is necessary to investigate that whether the semi-empirical XFLR5 software and the more traditional CFD software, like ANSYS Fluent, can both predict a similar aerodynamic performance of the UAV.

Furthermore, XFLR5 is known to provide satisfactory preliminary simulations (discussed below), but unfortunately it is limited to fluid simulations, which means that although the aerodynamic performance of a UAV can be estimated, it is not possible to predict the UAV's structural response from certain flight conditions. Because of this, it is also vital to investigate the structural integrity of both wings under two types of typical flight conditions: comparing airspeed of 13 m s^{-1} (*normal*

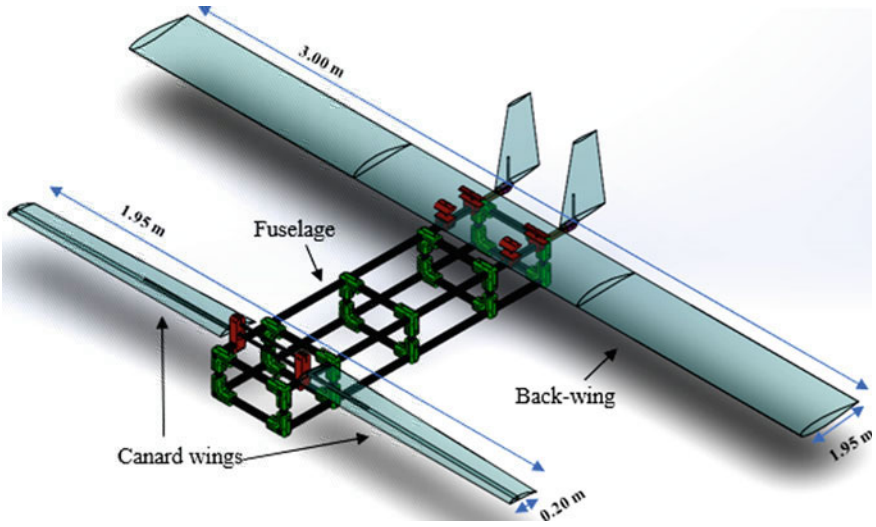

Fig. 1 Present study's Computer-Aided Design (CAD) model

Table 1 Material used in present study

Component	Material
Wings' materials[a]	Woven and unidirectional Carbon Fibre Reinforced Plastic (CFRP); woven Glass-Fibre reinforced Plastic (GFP); Expanded Polypropylene (EPP) foam
Wing-fuselage connector's materials[a]	PETG (3D printed); aluminum alloy bolt

[a]Materials used in the wings and connector are obtained from the student team (Haggis Aerospace) in charge of the UAV [1], but data owned by the author K. Marangi

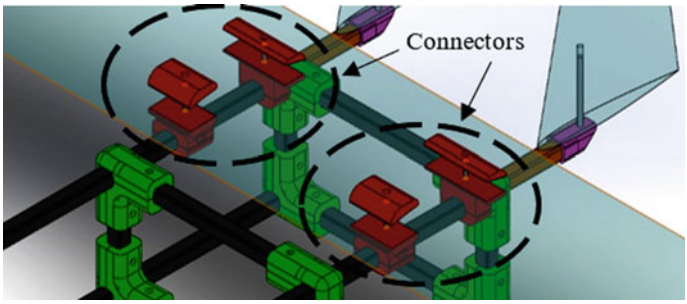

Fig. 2 Close-up view of the components connecting the back-wing and the fuselage

flight condition) to airspeed of 23 m s^{-1} (*wind gust* flight condition). Predicting the structural consequences of a wind gust is beneficial as it would evaluate the current structural performance of the UAV, which would prevent critical damage during flight due to unforeseen airspeed changes. A one-way FSI is employed to carry out this investigation, which is done by coupling CFD and FEA. Table 1 lists the main materials that will be considered in this study. The majority of the components were manufactured using composite materials, except from the back-wing's wing-fuselage connectors using Polyethylene Terephthalate Glycol-modified (PETG) and aluminium nutted bolts to provide clamping power (Fig. 2).

In the present study, ANSYS FLUENT is used to first simulate the airflow around the wings of the UAV for the different wind speeds, providing a large amount of information about the corresponding airflows, such as pressure fields which are flow necessary properties for a FSI analysis.

These pressure fields were then transferred to ANSYS MECHANICAL and mapped onto the structural model of the UAV wings to investigate the resulting stresses. For this stage, the wings are modelled as a 3D cantilever with varying loading, as well as with a fixed end at the wing root. It was also necessary to account for the fact that the wings are manufactured using several materials.

Lastly, in order to analytically determine the stresses on the wing-fuselage connectors, the previously numerically calculated wing stresses obtained from the previous stages are implemented into the analytical problem. It was possible to simplify this connector problem to a simple tensile stress problem thanks to several assumptions

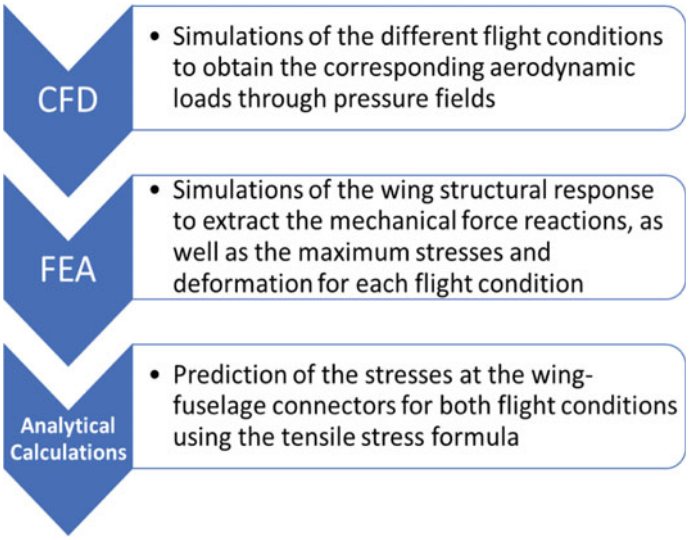

Fig. 3 Present study's workflow

which are going to be presented in the Methodology section. Figure 3 summarises the workflow for the present study, which also builds on from previous work [2].

UAVs generally operate at lower Reynolds number (~10^5) than larger transonic commercial aircrafts (~10^8), due to their reduced size and operating velocity. Inertial forces are still dominant in the flow at this Reynold number range, which is the reason why turbulence still needs to be considered in the computational problem. This modelling is achieved in CFD software through turbulence closure schemes. In fact, *Spalart-Allmaras* (SA) and *k-ω SST* are two turbulence models which were applied to external aerodynamics problems. For instance, Panagiotou et al. [3] used *SA* in their UAV aerodynamic analysis, while Kontogiannis et al. [4] employed *k-ω SST*. The versatility between the two models is due to the fact that the former was specifically developed for the aerospace industry [5], and the latter is known to have satisfactory performance in transitional and low Reynolds number flows [6]. As the UAVs from the above-mentioned studies featured a more traditional wing configuration, the present study employs both of these two turbulence models to evaluate their performance on a UAV with a canard wing configuration, whose respective results were then compared against validation data obtained with the semi-empirical XFLR5 software.

Studies by Kanesan et al. [7] and Ramos [8] have verified FEA predictions of the structural performance of winds to external forces. The present study adopted the same procedures outlined in these previous investigations due to the shared similarities including boundary conditions and material selection.

The FSI analysis for different flight conditions—23 and 13 m s^{-1} for *wind gust* and *normal* flight conditions, respectively—provides sufficient information to predict the

structural performance of the UAV wings and wing-fuselage connectors, ensuring that a sudden wind gust would not lead to a catastrophic in-flight failure of the UAV.

2 Methodology

The following section presents the present study's methodology to perform a FSI simulation: first, flow simulations are obtained through CFD, which are then coupled with structural analysis through FEA. The methodology to predict the stresses in the wing-fuselage connectors through analytical calculations is also explained last.

2.1 Fluid Simulation Using CFD

The procedure that is employed to carry out the flow simulation is now described. A half-body computational domain is used due to symmetry in the geometry of the wings, as shown in Fig. 4 to enhance the mesh resolution while balancing computational cost. The generated domain is made of approximately 3 million cells (Fig. 5), with inflation layers having a $y^+ = 1$, in order to guarantee that the boundary layer phenomenon is captured adequately as described in previous studies [3, 4, 9, 10].

Table 2 summarises the employed boundary conditions for the flow simulation. Two flight-conditions: *normal* and *wind gust* are studied corresponding to two different inlet velocities. The resultant pressure fields are used in the subsequent structural analysis. Ultimately, the goal is to determine whether the UAV wings will be able to withstand the additional stresses introduced by an increase in airspeed.

The flow field is determined with the *SA* and *k-ω SST* turbulence models, which was already presented earlier in this study. The aerodynamic wing loading is obtained through the numerically calculated pressure distribution.

To validate the CFD results, the same geometry and boundary conditions are tested using the semi-empirical CFD software XFLR5 in order to compare the numerical results against those obtained from ANSYS. XFLR5 is considered a viable alternative in the absence of experiments. The software has been benchmarked against experimental results in the past with overall satisfactory prediction [11, 12]. A separate study has not only demonstrated XFLR5's capability to accurately simulate low Reynolds numbers flows but has also shown its widespread use in flow simulations regarding a range of airfoil-dependent investigations [13].

2.2 Structural Analysis

Composite materials are used to manufacture the wings as shown in the CAD model in Fig. 6. The back-wing comprises of a EPP foam core shelled by a 3 mm thick

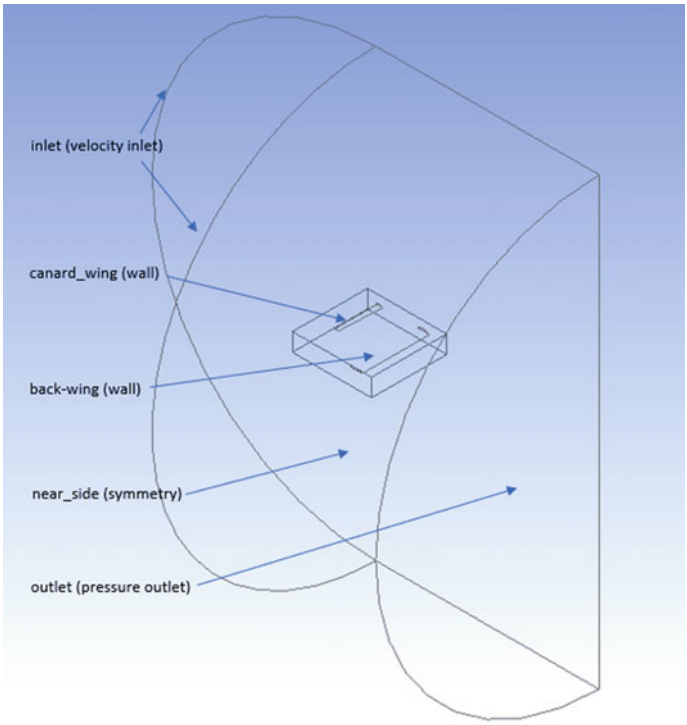

Fig. 4 Computational domain employed for flow simulation in ANSYS Fluent (CFD)

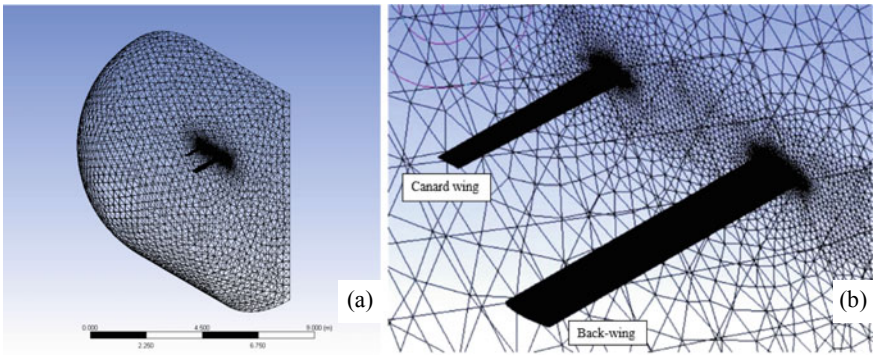

Fig. 5 CFD computational grid: **a** isometric view; **b** close-up view of mesh refinement in the vicinity of the wings

Table 2 Boundary conditions for flow simulations

Boundary name	Boundary type	Boundary conditions
Inlet	Velocity inlet	p = 0 atm (gauge pressure); T = 300 K; $v_1 = 13$ m s^{-1} (*normal state*); $v_2 = 23$ m s^{-1} (*wind gust*); Angle of incidence = 3.0°
Near side	Symmetry	Symmetrical with respect to boundary
Canard wing; Back-wing	Wall	v = 0 m s^{-1} (no-slip condition)
Outlet	Pressure outlet	–

Cf. Fig. 4 for the various boundary locations

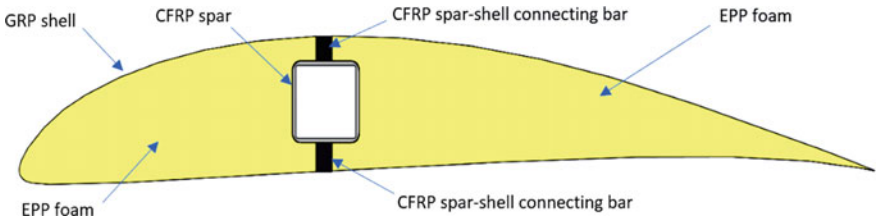

Fig. 6 Back-wing's wingroot cross-section—by Haggis Aerospace [1] but owned by the author K. Marangi

hand-laminated GRP, with a CFRP tube running through the location where the wing is at its thickest. The CFRP tube acts as the wing's spar and is designed to absorb the aerodynamical loads transmitted from the outer part of the wings. Unidirectional CFRP bars are employed to convey the torsional moment from the wings' skin to the CFRP tubes [14].

Pressure fields are extracted from the flow simulations in ANSYS FLUENT and are then mapped onto the wings' equivalent structural models in ANSYS MECHANICAL. This stage is where the coupling between CFD and FEA occurs, or in other words, where the fluid flow problem is converted into a structural one.

The anisotropic mechanical properties of the various materials illustrated in Fig. 6 (Young's Modulus *Ex Ey Ez* & Poisson's ratio ν_{xy}, ν_{yz}, ν_{xz} are listed in Table 3. These are extracted from ANSYS' Material Library [15].

2.3 Analytical Analysis

The back-wing connectors (Fig. 2) are modelled with a number of assumptions to facilitate the analytical calculations of the resulting stresses. The connectors comprise of two components: the 3D printed parts and the M4 bolts (cf. Table 1). The following assumptions are made for the analytical calculations:

Table 3 Mechanical properties of wings' materials

Parameter	Glass fibre Reinforced Plastic (woven, wet)	Carbon Fibre Reinforced Plastic (woven, wet)	Carbon Fibre Reinforced Plastic (UD, wet)
Ex (MPa)	35,000	59,160	1.23×10^5
Ey (MPa)	9000	59,160	7780
Ez (MPa)	9000	7500	7780
ν_{xy}	0.28	0.04	0.27
ν_{yz}	0.4	0.3	0.42
ν_{xz}	0.28	0.3	0.27

Table 4 Mechanical properties of the aluminum alloy bolt, assuming material homogeneity and isotropy

Parameter	Value
Young's Modulus (GPa)	72
Yield strength (MPa)	505

- The front connectors are located above the wing's neutral point (the entire generated aerodynamic load is applied to this fixed region);
- The aerodynamic load is directly applied to the connectors nutted bolts, which provide the necessary clamping power;
- The drag force is ignored because it is negligible compared to the lift force experience;
- The mechanics of the fasteners are not considered, and the stress limits of the bolt material [16] is set as the determining factor (assuming homogeneity and isotropy of the bolt) (Table 4).

Based on these assumptions, it is possible to calculate the resultant tensile stresses in the connectors M4 bolts for the two different flight conditions using the Formula (1) [where σ is the resulting stress (Pa), F is the applied force (N), & A the item's cross-sectional area (m^2)].

$$\sigma = \frac{F}{A} \tag{1}$$

3 Results and Discussions

This section presents the results from the FSI simulations, starting with the CFD and FEA results, then ending with the analytical calculations.

3.1 Flow Simulation

The generated aerodynamic loads (lift and drag) from the CFD simulations are presented in Table 5.

For the *normal* wind condition, ANSYS predicted a sensible lift force as one would expect in scenarios where the UAV reaches level-flight. This implies that the lift and the weight - two vertical opposing forces—are cancel each other out. For the normal flight condition, the total lift forces are 77.2 N using *k-ω SST*, and 77.8 N using *SA*. It is possible to partially validate the CFD results from the ANSYS-predicted lift forces as these correspond to typical level-flight cases for this type of UAV.

For the *wing gust* condition, *k-ω SST* and *SA* obtained similar total lift values of 244 N and 246 N, respectively. These values imply that there has been an increase of 216% in aerodynamic forces due to the sudden acceleration experienced by the UAV. Nevertheless, this significant rise in lift is expected, as the vehicle's velocity is a squared term in the lift Formula (2) [where ρ is the air's density (Pa), v the airspeed (ms^{-1}), S the projected wing area (m^2), and C_L the lift coefficient].

$$L = \frac{1}{2}\rho v^2 S C_L \tag{2}$$

Regarding the different values presented in Table 5, both turbulence closure schemes obtained similar lift results, with less than 1% error in both flight conditions. In fact, there is a 0.78% error between *k-ω SST* and *SA* for *normal* conditions and 0.82% for *wind gust* conditions. These minor discrepancies imply that either turbulence model is suitable to their similar performance.

To validate the numerical results, the numerical results produced by *k-ω SST* and *SA* in ANSYS FLUENT are compared against values generated by XFLR5, which is displayed in Table 6 for the aerodynamic coefficients. From this table, the drag coefficient is unanimously predicted to have a value of 0.05, although there is an approximate 20% difference between ANSYS and XFLR5 results in terms of lift coefficient. Taking into account that the lift coefficient is calculated from the lift Formula (2) shown above, this discrepancy could be explained by the fact that the

Table 5 Generated aerodynamic loads for the two flight conditions

Parameter	Value	
Normal conditions ($V = 13\ ms^{-1}$)		
Turbulence model	*k-ω* SST	SA
Lift force (N)	77.2	77.8
Drag force (N)	4.34	4.04
Wind gust conditions ($V = 23\ ms^{-1}$)		
Turbulence model	*k-ω* SST	SA
Lift force (N)	244	246
Drag force (N)	13.2	13.2

Table 6 Aerodynamic coefficients from CFD simulations

Parameter	Value		
	k-ω SST	SA	XFLR5[a]
Lift coefficient	0.96	0.97	0.76
Drag coefficient	0.05	0.05	0.05

[a]XFLR5 values obtained from the student team (Haggis Aerospace) in charge of the UAV [1]. Data owned by the author K. Marangi

other variables of the formula had different values when calculated in XFLR5. These differences could be related to the air viscosity or density.

Figures 7 and 8 provide qualitative results of the flow simulations for both flight conditions based on the results from k-ω *SST* (note that both turbulence models performed similarly). In these figures, the pressure coefficients across the wings' surfaces are depicted through contours. These coefficients describe the relative pressures throughout a specific flow field, based on Eq. (3) [where C_p is the pressure coefficient, p the static pressure at a specific location (Pa), p_∞ the freestream static pressure (Pa), p_0 the freestream stagnation pressure (Pa), ρ_∞ the freestream fluid density (kg m^{-3}) & V_∞ the plane's velocity (m s^{-1})].

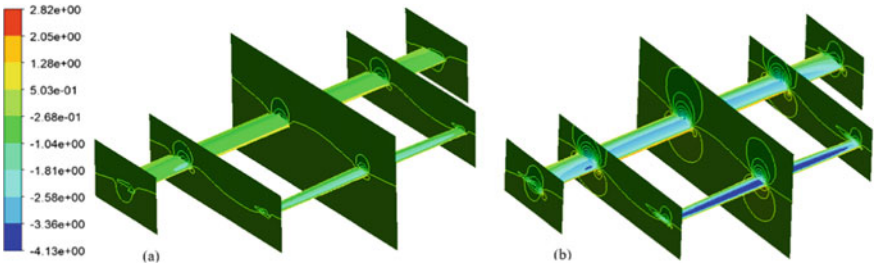

Fig. 7 Pressure coefficient contours for: **a** normal, 13 ms^{-1} and **b** wind gust, 23 ms^{-1} flight conditions

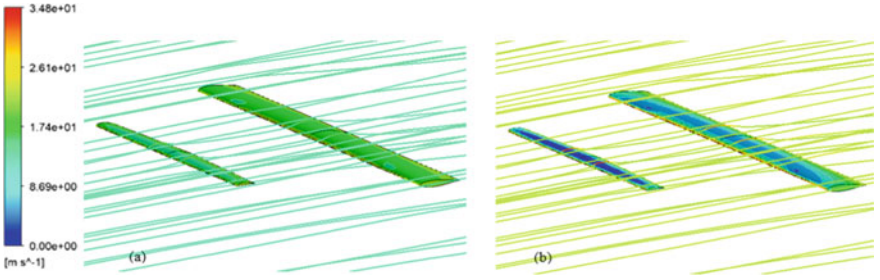

Fig. 8 Streamlines and pressure coefficient contours for: **a** normal 13 ms^{-1}, and **b** wind gust 23 ms^{-1}, flight conditions

$$C_p = \frac{p - p_\infty}{\frac{1}{2}\rho_\infty V_\infty^2} = \frac{p - p_\infty}{p_0 - p_\infty} \tag{3}$$

In Fig. 7, the contours generally show low values of pressure coefficient on the upper wing surfaces compared to higher values on the lower surfaces. An upward lifting force is generated as a result of this pressure difference. Comparing the *wind gust* (Fig. 7b) against the *normal* conditions (Fig. 7a), a larger pressure difference is observed and as a consequence greater aerodynamic loads are experienced. This agrees with the information found in Tables 5 and 6. Moreover, Fig. 8 demonstrates that the airflow on the upper wing surfaces has the largest velocity, which agrees with Bernoulli's principle: the faster the flow, the lower its pressure.

The flow simulation results from ANSYS CFD, specifically the pressure fields, are exported to ANSYS Mechanical to carry out the second step.

3.2 Structural Analysis

The structural investigation is executed in two stages. Firstly, static FEA simulations in ANSYS Mechanical predict the wing stresses due to aerodynamic loads. In the second step, the reaction forces obtained in the FEA simulation are used to analytically calculate the resultant stresses induced at the wing-fuselage connectors from the aerodynamic loads.

Table 7 summarises the results from ANSYS Mechanical for each of the wings during both flight conditions.

The largest magnitude of the maximum stress is experienced on the back-wing, with values of 75.0 MPa during *wind gust* and 23.8 MPa during *normal* condition.

Figure 9 illustrates the maximum equivalent stresses. The largest stresses are concentrated on the back-wing spar-shell connecting bar (labelled 'max' on Fig. 9b).

Table 7 Results from ANSYS mechanical

Parameter	Value	
Wing	Canard	Back
Flight conditions	*Normal* ($v_1 = 13$ ms^{-1})	
Maximum Stress (MPa)	3.30	23.8
Reaction Force (N)	13.5	25.0
Maximum Deformation ($\times 10^{-3}$ m)	3.00	0.70
Flight conditions	*Wind gust* ($v_2 = 23$ ms^{-1})	
Maximum stress (MPa)	10.0	75.0
Reaction force (N)	42.2	78.9
Maximum Deformation ($\times 10^{-3}$ m)	9.50	2.25

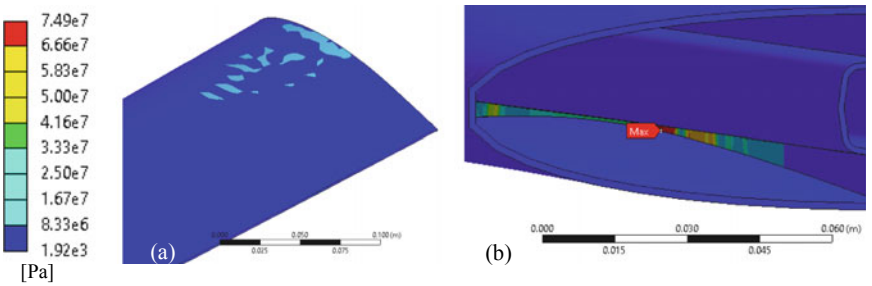

Fig. 9 Equivalent stress contours of **a** canard wing and **b** back-wing (close-up view on regions of high stresses for each wing)

To determine whether these high stresses pose a risk of damage the maximum stress failure criteria was employed. The maximum stress failure criteria is based on non-interactive theory [17], which does not take consider the interaction between the different composite elements. The computed stress is then evaluated against the component's material stress limit. The computed stresses are compared to the orthotropic stress limits and are below the tensile limit of 1632 MPa and compressive limit of −704 MPa (cf. Table 3).

The ANSYS Mechanical reaction forces for each flight condition are exported as inputs in the tensile stress Formula (1) for the investigation of the transmitted stresses to the wing-fuselage connector. These are presented in Table 8. The M4 bolt experiences a tensile stress of 1.98 MPa during *normal* conditions, increasing to 5.95 MPa during the *wind gust*. These stresses are below the bolt yield strength of 505 MPa, producing a factor of safety of 85. This implies that the implemented connector design is satisfactory and will not fail under the assumed flight conditions.

Finally, Fig. 10 illustrates the resultant deformation for the two flight conditions. From Table 7, it is observed that the canard wing experiences the largest deflection with a value of 3.00 mm during *normal* flight condition, increasing to 9.5 mm during the *wind gust* (an increase by a factor of 3). This could be explained by the fact that the canard lacks a component connecting its GRP shell to its spar, and therefore the shell takes on the entire stresses from the aerodynamic lifting force.

Table 8 Results from Analytical analysis

Parameter	Value	
Flight condition	Normal ($v_1 = 13$ ms^{-1})	Wind gust ($v_2 = 23$ ms^{-1})
Cross-sectional area (m^2)	1.26×10^{-3}	
Applied Force (N)	25.0	78.9
Resultant Stress (MPa)	1.98	5.95

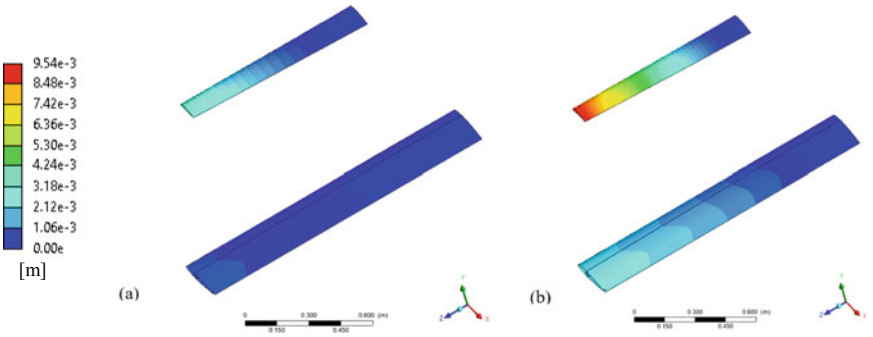

Fig. 10 Total deformation contours on wings for: **a** normal (13 ms^{-1}) and **b** wind gust (23 ms^{-1}) flight conditions

4 Conclusion

The present study examines the structural integrity of the wings and wing-fuselage connectors of a UAV exposed to varying aerodynamic loads during two different flight conditions using Fluid-Structure Interactions. ANSYS FLUENT is first used to numerically simulate the airflow around the wings. The resultant pressure fields are imported into ANSYS MECHANICAL to carry out a static structural analysis (FEA). The wings' deformation and maximum stresses due the aerodynamic loads are predicted. Lastly, the stresses in the back-wing's wing-fuselage connector are calculated analytically, and the maximum stress failure criteria is applied.

It is observed that the pressure differential between the upper and lower surfaces of the wings is much larger during *wind gust* compared to *normal* condition due to the increase in airspeed. Consequently, the aerodynamic forces increased as well, leading to significant larger stresses and to deformations (by a factor of 3). However, these resultant stresses were still below the limits by a very safe margin.

The FSI simulations that were presented in this study can be applied to related studies as it allows engineers to evaluate the aerodynamic and structural performance of a mechanical system without the need of a physical prototype, which is often costly and time-consuming to implement.

Acknowledgements We thank the University of Dundee's engineering student team participating in the *IMechE UAS Challenge* competition—HAGGIS AEROSPACE—and Dr. Triantafyllos Gkikopoulos (RaptorUAS) for suggesting this research title and for the insightful discussions on UAVs. We would like to also thank the Institution of Mechanical Engineers for supporting us in the participation of the IAENG 2019 conference.

References

1. Haggis Aerospace, *Critical Design Review*. Document submitted for IMechE UAS Competition 2017, Dundee (2017)
2. K. Marangi, S. M. Salim, Predicting the structural performance of the wings of an unmanned aircraft vehicle using fluid-structure interaction, in *Lecture Notes in Engineering and Computer Science: Proceedings of The World Congress on Engineering 2019*, London, UK, 3–5 July 2019, pp. 500–505
3. P. Panagiotou, P. Kaparos, C. Salpingidou, K. Yakinthos, Aerodynamic design of a MALE UAV. Aerosp. Sci. Technol. **50**, 127–138 (2016)
4. S. Kontogiannis, D. Mazarakos, V. Kostopoulos, ATLAS IV wing aerodynamic design: from conceptual approach to detailed optimization. Aerosp. Sci. Technol. **56**, 135–147 (2016)
5. P. Spalart, S. Allmaras, A one-equation turbulence model for aerodynamic flows, in *30th Aerospace Sciences Meeting and Exhibit* (1992)
6. S. Kontogiannis, J. Ekaterinaris, Design, performance evaluation and optimization of a UAV. Aerosp. Sci. Technol. **29**(1), 339–350 (2013)
7. G. Kanesan, S. Mansor, A. Abdul-Latif, Validation of UAV wing structural model for finite element analysis. Jurnal Teknologi **71**(2) (2014)
8. M. Ramos, Construction and analysis of a lightweight UAV wing prototype, M.S thesis, Técnico Lisboa, Lisbon, Portugal (2015)
9. S.M. Salim, S.C. Cheah, Wall y^+ strategy for dealing with wall-bounded turbulent flows, in *Proceedings of International MultiConference of Engineers and Computer Scientists*, vol. 2 (2009), pp. 2165–2170
10. S.M. Salim, M. Ariff, S.C. Cheah, Wall y^+ approach for dealing with turbulent flows over a wall mounted cube. Prog. Comput. Fluid Dyn. **10**(5–6), 341–351 (2010)
11. A. Deperrois, About XFLR5 calculations and experimental measurements (2009). [ebook]. Available http://www.xflr5.com/docs/Results_vs_Prediction.pdf
12. J. Morgado, R. Vizinho, M. Silvestre, J. Páscoa, XFOIL vs CFD performance predictions for high lift low Reynolds number airfoils. Aerosp. Sci. Technol. **52**, 207–214 (2016)
13. XFLR5, Xflr5.com (2018). (Online). Available http://www.xflr5.com/xflr5.htm. Accessed 2 Nov 2017
14. M. Simons, *Aerodynamics of model aircraft flight*, 5th edn. (Special Interest Model Books Ltd, Dorset, England, 2015)
15. Workench Mechanical. Ansys
16. Aluminum Socket Cap Bolt M4 x (0.7 mm) x 20 mm, Pro-bolt.com, 2015. (Online). Available https://www.pro-bolt.com/aluminium-allen-bolt-m4-x-0-7mm-x-20mm-21.html. Accessed 5 Mar 2018
17. N. Tiwari, *Introduction to Composite Materials and Structures: Strength of a Composite Lamina* (2018). [ebook] Available https://nptel.ac.in/courses/112104168/L32.pdf

A Vision Guided Robot for Gluing Operations

Stefano Pagano, Riccardo Russo, and Sergio Savino

Abstract The paper describes the development of an automatic machine to be adopted to glue the shoe upper to its sole or to glue a rubber insert on the lower surface of the sole. The machine prototype consists in a cartesian robot that drives a glue gun and by a vision system that can recognize the sole, placed on a worktop, allowing the planning of the glue gun trajectory. After a description of the machine hardware assembly, the developed procedures that allows the sole recognition and the robot planning trajectories are presented. Finally, the results of several tests, performed to check the procedure goodness, are reported.

Keywords Arduino · Automatic machine · Footwear manufacturing · Gluing process · Soles · Vision sensor

1 Introduction

In the last 50 years, shoes have undergone considerable evolution, both in terms of materials and fixing systems for their parts; in a recent past, the soles were mainly made of leather, sometimes with rubber inserts placed on the lower surface and the upper was fixed to the sole by means of hooks and seam.

Currently, the large series production provides shoes made with increasingly lighter materials and equipped with soles made of deformable material that are, at the same time, comfortable, breathable, durable and able to provide good thermal protection. Great importance is given to the sole cushioning function, especially for sports shoes that, in some cases, are equipped with gas-filled bag, inserted in the sole

S. Pagano (✉) · R. Russo · S. Savino
Dipartimento di Ingegneria Industriale, Università degli Studi di Napoli Federico II, via Claudio n.21, 80125 Naples, Italy
e-mail: pagano@unina.it

R. Russo
e-mail: riccardo.russo@unina.it

S. Savino
e-mail: sergio.savino@unina.it

S.-I. Ao et al. (eds.), *Transactions on Engineering Technologies*,
https://doi.org/10.1007/978-981-15-8273-8_2

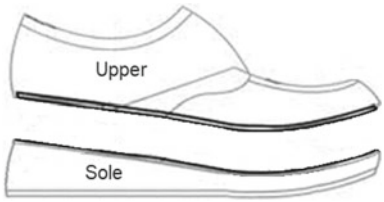

Fig. 1 Shoe upper and sole

to prevents impacts [1]. Therefore, in addition to traditional leather soles, there is a vast production of synthetic materials soles belonging to the following groups or their combination [2, 3]:

- thermoplastic rubber (TPR) and thermoplastic polyurethane (TPU);
- two-component polyurethane materials: polyether-based PUR, polyester-based PUR;
- copolymers such as rubber and EVA (Ethylene vinyl acetate).

The soles for footwear must comply with the requirements indicated by various international standards to be labeled as quality sole.

The standard establishes the tests to be performed to assess resistance to bending, abrasion, de-lamination, slip, water penetration, dimensional stability, compressive and splitting tensile strength, of the stitching point and to bonding capacity.

When uppers and soles (Fig. 1) are joined by gluing, the junction zone is subject to a combination of tensile, shear and peel stresses; the most critical stress is the peel one. For this reason, special instruments are adopted to test the adhesion strength between upper and sole. The load causing the separation can be measured or alternatively, a pass load can be applied to check that the adhesion is satisfactory. This second operation method is the more adopted in the shoe factory since it can be applied to the ordinary shoes of the production lines.

In the standard EN 15307 there are reported the minimum shoes peel strength for different kind of shoe. For example, it must be greater than 3.0 N/mm^2 for men town footwear; 2.5 N/mm^2 for women town footwear; 5.0 N/mm^2 for mountain footwear.

This paper refers about the development of a gluing machine prototype, called Ulisse [4] that allows to connect uppers and rubber inserts to the soles; the gluing operation must be carried out with great care in order to meet the current standards of resistance; at the same time, it must be carried out as quickly as possible to contain production costs. The automatic machine prototype uses a vision system to recognize the sole on which the glue must be dispensed, allowing to plan the trajectory of a cartesian robot that drives the glue gun. It was implemented with procedures that allow to compensate for mechanical misalignments between robot and vision system and to identify some particularities of the soles such as tapered edges or raised edges [5]. Some preliminary tests are reported in [6].

The developed prototype improves all the parameters of the production tetrahedron. In fact, it allows to improve:

(a) the production *costs*. The machine may be produced by means of cheap preassembled components and does not require operators having specific skills;
(b) production *time*. The developed procedures allow to arrange the soles to be glued in an arbitrary position on the worktop and does not require preliminary operations such as storing the sole geometry;
(c) production *flexibility*. The prototype can operate on soles having different sizes and shapes;
(d) production *quality*. It is possible to control the amount of glue dispensed by adjusting the glue gun velocity, the distance from the object and the glue flow rate, allowing to guarantee the required adhesion resistance.

2 Prototype Description

The gluing machine prototype (Fig. 2) was made with pre-assembled and low-cost elements. It mainly consists of a closed cabin containing a worktop on which are placed the soles to be glued; a vision system able to recognize the shape of the soles; a Cartesian robot whose end-effector is a glue gun; an aspirator, placed under the worktop, to suck the glue vapors avoiding their dispersion in the work environment. The main components of the machine are described in detail below.

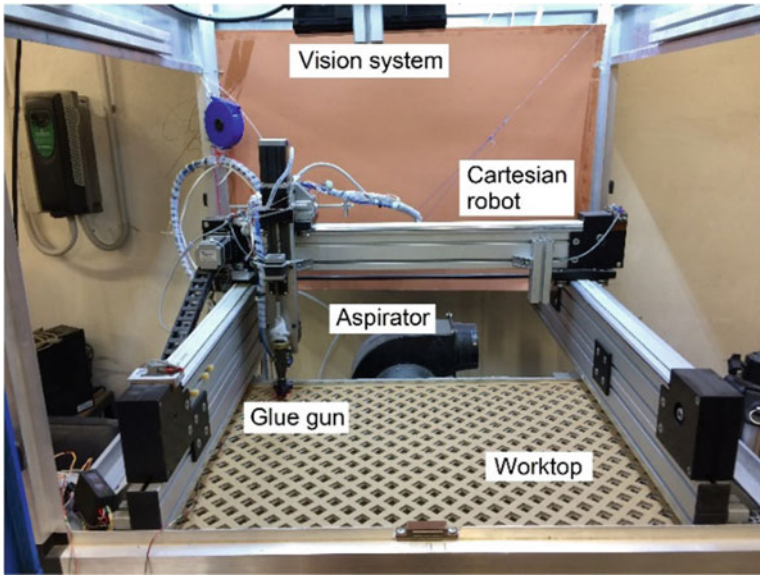

Fig. 2 Gluing machine prototype